Phase Separation, Crystallization, and Structure Formation in Immiscible Polymer Solutions

J. L. ZRYD and W. R. BURGHARDT*

Department of Chemical Engineering, Northwestern University, Evanston, Illinois 60208

SYNOPSIS

Morphological and calorimetric studies of phase separation have been carried out in solutions of a crystallizable polymer in poor solvents. Hydrogenated polybutadiene with low branch content was investigated in solutions with diphenyl ether and diphenyl methane, in which the equilibrium phase diagram exhibits both liquid–liquid phase separation and crystallization of the polymer. Emphasis is placed on sample preparation protocols using thermal treatments at low concentrations where it is anticipated that both phase separation mechanisms may influence the resulting morphology. Samples prepared using either ramp cooling or isothermal crystallization exhibit porous structures such as those seen in membrane materials, that predominantly reflect liquid phase separation. However, the interplay between the different kinetics of liquid demixing and crystallization provides a mechanism to control, for instance, pore size. DSC studies during ramp cooling showed evidence of two discrete crystallization processes associated with the two liquid phases expected to be present under these circumstances. Finally, high concentration samples showed morphological evidence of liquid phase separation induced at the growth front of spherulites in otherwise single-phase polymer solutions. © 1995 John Wiley & Sons, Inc.

INTRODUCTION

Phase separation processes and the resulting multiphase morphology play a critical role in determining the physical properties of polymeric materials. In some cases, phase separation is directly responsible for useful and/or unique properties for specific applications. An outstanding example is the formation of microporous polymer membranes from polymer solutions. Liquid demixing can lead to a porous, interconnected structure, where the open pores in the final membrane product correspond to the polymer-lean phase formed during phase separation. Commercial membranes are typically produced by phase inversion,[1] in which a thin film of polymer solution is coagulated by quenching into a nonsolvent; exchange of solvent and nonsolvent by diffusion within the film moves the solution into a two-phase region on the ternary phase diagram. An alternative strategy that has received much interest is the thermally induced phase separation (TIPS) process,[2-21] where thin films of polymer solutions in marginal solvents are cooled from the one-phase to the two-phase region of the phase diagram.

Greater understanding of the phase separation phenomena that occur in membrane formation can lead to improved processing strategies. Toward this end, the TIPS procedure offers advantages for systematically probing the relationship between phase separation and membrane morphology, since the "process path" on the phase diagram is subject to external control, through temperature. Conversely, concentration profiles in phase inversion evolve via mass transfer during the quench step without an opportunity for direct intervention. Most studies along these lines have focused exclusively on systems which exhibit only one type of phase separation. These include liquid–liquid demixing in amorphous polymers,[3-10] in which the role of the phase separation mechanism (spinodal decomposition vs. nucleation and growth) is explored along with subsequent coarsening in the phase-separated solution to determine membrane morphology and pore size. Typically, evolution of the two-phase structure is

* To whom correspondence should be addressed.

Journal of Applied Polymer Science, Vol. 57, 1525–1537 (1995)
 CCC 0021-8995/95/121525-13

arrested by a rapid temperature quench to a temperature at which the solvent crystallizes, or the polymer-rich phase vitrifies. Other studies have investigated liquid–solid phase separation during crystallization of the polymer and/or the solvent from a one phase solution.[11-17] Crystalline polymers in marginal solvents provide yet another alternative for the formation and solidification of membrane structure.[16-23]

The opportunity for polymer crystallization dramatically changes the nature of the equilibrium phase diagram for membrane-forming systems with limited liquid miscibility, both in ternary polymer–solvent–nonsolvent[22,23] and binary polymer–solvent systems.[24] Figure 1 shows a schematic phase diagram for a binary polymer solution that exhibits both liquid–liquid demixing and polymer crystallization. The crystal saturation curve representing melting point depression defines a region of equilibrium between a pure polymer crystal and liquid phase. At low concentrations, typical UCST phase behavior is observed, where the binodal curve defines equilibrium concentrations of two coexisting liquid phases. At the intersection of the binodal and crystal saturation curves, a three-phase point (monotectic) emerges. Below this temperature, the lowest free energy state is pure crystal in equilibrium with a dilute polymer solution. Thus, the majority of the equilibrium phase diagram is dominated by crystal–liquid equilibrium.

There are extensive reports of phase diagrams analogous to Figure 1 for solutions of crystallizable polymers in poor solvents.[25-33] The shape of the phase diagram is strongly influenced by solvent

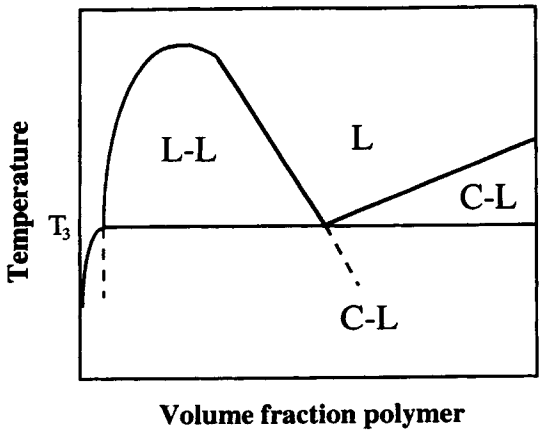

Figure 1 Typical solution phase diagram for crystallizable polymer in a poor solvent, showing regions of liquid–liquid (L–L) and crystal–liquid (C–L) equilibrium. Binodal curve extended below the three phase point has no equilibrium significance.

quality and molecular weight, primarily by shifting the binodal vertically. These factors have relatively little impact on the crystal saturation curve, however. Even though the equilibrium phase diagram is dominated by crystallization, the dynamics of phase separation may be strongly influenced by liquid phase separation, since formation of a stable nucleus for crystallization may be much slower than liquid demixing. As an extreme example, Lee et al.[31] observed cloud points reflecting liquid phase separation at temperatures *below* the crystal saturation curve by systematically varying χ in i-PP solutions. Although there is no region of liquid–liquid coexistence in the *equilibrium* phase diagram, a region of liquid instability may be accessed by suitably fast cooling. Similar "hidden" binodals may be responsible for morphologies characteristic of liquid demixing observed in rapidly quenched solutions of i-PP in eicosanoic acid by Kim and Lloyd,[17,34] and have been invoked by Aubert to explain peculiar morphologies in physical gelation of i-PS solutions.[35]

More generally, in the presence of two competing phase separation mechanisms it is expected that kinetic effects may have a dramatic influence on the resulting morphology. Since crystallization rates are strongly dependent on undercooling, it is possible that subtle changes in thermal history may result in significant changes in morphology or pore size of the resulting porous structure. In this work we systematically study the competition between these two phase separation mechanisms, and its influence on phase-separated morphology. We study an analog of polyethylene, hydrogenated polybutadiene with low branch content, since anionic synthesis allows for control over molecular weight and polydispersity. Polyethylene solutions formed in diphenyl ether and diphenyl methane are known to exhibit phase behavior illustrated in Figure 1.[27] Our approach is to subject homogeneous solutions to well-defined thermal histories and to study the resulting phase-separated structures using optical and electron microscopy. In addition, DSC is used to study the crystallization and melting behavior, both during and following the prescribed thermal treatments. Limited experiments were also performed using xylene as a solvent to examine crystallization in a system that does not exhibit liquid demixing.

EXPERIMENTAL

Materials

Polybutadiene was anionically polymerized in cyclohexane. The reaction was performed at room

temperature with *sec*-butyl lithium as the initiator using a "capped bottle" technique as previously described.[36] Characterization of the polybutadiene was carried out prior to hydrogenation. Gel permeation chromatography (GPC) was performed at 40°C in THF. Analysis using Mark-Houwink parameters[37] $K = 3.23 \times 10^{-4}$ g/dL and $a = 0.72$ yielded $\overline{M}_w = 60{,}000$ with a polydispersity of 1.2. The branch content (due to 1–2 additions) was determined using infrared spectroscopy (IR) to be approximately 17 ethyl branches per 1000 main chain C atoms. Hydrogenation was performed in cyclohexane at 500 psi with palladium on calcium carbonate as the catalyst using established procedures.[38] Saturation was confirmed using IR. Diphenyl ether and diphenyl methane solvents (99% + purity) were purchased from Aldrich Chemical Co., and xylene (certified ACS grade) was purchased from Fisher Scientific. All solvents were used as received.

Methods

Phase transitions were measured using a cloud point procedure, optical microscopy, and differential scanning calorimetry (DSC). The cloud point curves for samples of less than 20% polymer were found by measuring intensity of laser light transmitted through the solutions during slow cooling (0.5°C/min). Solutions were prepared by adding polymer and solvent to a test tube, sealing to prevent evaporation, and mixing at 150°C using a hot plate and magnetic stir bar. The cloud point was taken as the onset of a decrease in laser intensity. For solutions of polymer greater than 20%, the cloud point was determined using optical microscopy. Samples were prepared by mixing the two components in DSC pans at 150°C, quenching the sample in liquid nitrogen, opening the pan, placing the sample between a glass slide and cover slip, and sealing with tape. Samples were cooled at rates between 1 and 10°C/min in a Mettler FP82 hot stage and were examined in a Nikon polarizing microscope under white light. The cloud point was taken as the temperature where the first sign of phase separation occurred under a magnification of 125. An intermediate concentration was studied using both cloud point methods with consistent results.

Crystallization and melting transitions were measured at cooling and heating rates of 10°C/min using a Perkin-Elmer DSC 7 calibrated with indium. Crystallization temperature varies significantly with cooling rate and 10°C/min was arbitrarily chosen to guide later morphology studies as to the temperature and composition ranges where both liquid–liquid phase separation and crystallization are likely to occur. Equilibrium melting temperatures could not be obtained due to difficulties in determining these temperatures in random copolymers.[39] DSC samples were prepared by sealing appropriate amounts of polymer and solvent in volatile sample pans. Each component was weighed on a balance with a resolution of 0.01 mg, facilitating accurate measurements of composition on small samples. Samples were held at 150°C for 10 min prior to cycling to ensure mixing. All compositions are reported on a volumetric basis.

SEM samples were prepared in sealed DSC pans. Ramp-cooled samples were prepared in the DSC, while isothermal crystallizations were performed by quickly immersing heated, single-phase samples into a thermostated oil bath held at the appropriate temperature. After treatment, the samples were removed from the pan, frozen in liquid nitrogen, fractured, and placed into benzene for about 4 days to extract the diphenyl methane and diphenyl ether. Following drying of the samples, they were sputter-coated with gold and examined in a Hitachi S-570 SEM. Optical microscopy was also performed on ramp-cooled samples. Samples were prepared as described for cloud point experiments, and were ramped one time only in the hot stage. Subsequent weighing after cooling revealed minimal solvent loss due to the high boiling points of the solvents. The maximum ramp speed was limited to 10°C/min in the hot stage. Samples were examined in a Nikon polarizing microscope under crossed polarizers and white light. Optical microscopy has the advantages that structures may be examined with the solvent present, and crystal structures may be observed under crossed polarizers. Duplicate ramp-cooled and isothermal samples were left in DSC pans unopened and heated at 10°C/min in the DSC to study melting behavior.

RESULTS AND DISCUSSION

Figure 2 shows temperature–composition diagrams for HPB in diphenyl ether and diphenyl methane. In line with previous results in polyethylene solutions,[27] diphenyl methane is seen to be a better solvent, exhibiting lower cloud point temperatures and consequently a smaller region of liquid phase separation. However, changes in χ do not alter the melting and crystallization transitions a great deal. At low polymer concentrations, melting points do not vary significantly with composition. This is consistent with the expected invariance of the equilibrium melting point, a consequence of the phase

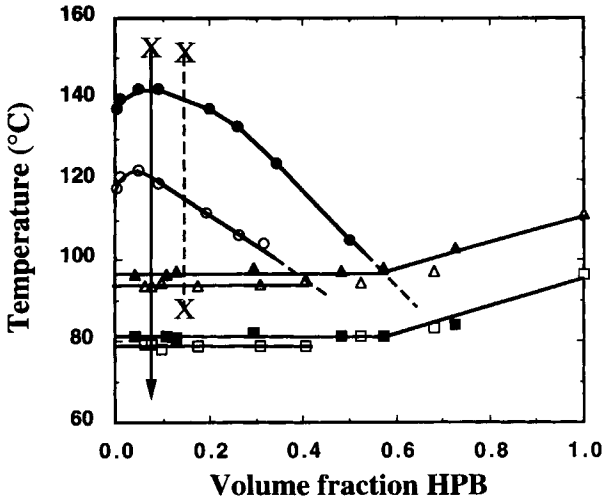

Figure 2 Experimental temperature–composition diagrams for diphenyl ether solutions (closed symbols) and diphenyl methane solutions (open symbols) of HPB. (○, ●) Cloud point; (△, ▲) DSC melting peak at 10°C/min; (□, ■) DSC crystallization peak at 10°C/min.

rule since crystals will melt at the three-phase point in this region of the phase diagram. However, such invariance is not always observed, which has been attributed to polydisperse polymer samples.[31,33] The melting and crystallization temperatures are highly sensitive to cooling and heating rates, while the cloud point curve is not. This highlights the fact that the relative rates of liquid phase separation and crystallization may vary considerably over a modest temperature range. While Figure 2 does not represent the equilibrium phase behavior for this system, it provides useful guidance as to the temperature and composition ranges where liquid demixing and crystallization will occur.

The two thermal histories that have been extensively employed are also represented schematically on Figure 2. In ramp coolings, a sample was first equilibrated in the one phase region of the phase diagram, and then subjected to a constant cooling rate, as illustrated by the solid arrow. In this case it is clear that liquid demixing should precede polymer crystallization. In isothermal treatments, represented by the dashed line, a sample was rapidly quenched from the one-phase region to an intermediate temperature where crystallization and liquid phase separation are both possible. Temperatures were selected based on the crystallization and melting transitions observed at 10°C/min in the DSC. At temperatures between these transitions, crystallization should occur over a time scale that changes dramatically as a function of undercooling. Unlike the ramp cooling where some liquid phase separation must precede crystallization, the isothermal treatments are designed so that direct competition between the two-phase separation mechanisms may be explored. Most morphological studies were carried out using concentrations of 10% HPB in diphenyl ether and 7% HPB in diphenyl methane. These concentrations are near the maxima in cloud point, and thus near the critical condition, where it is expected that the early stages of liquid–liquid phase separation should occur by spinodal decomposition. Other concentrations were also studied to investigate the effect of composition on morphology or crystallization/melting behavior.

Ramp Treatments

Figure 3 presents typical structures seen after ramp cooling using both optical microscopy and SEM. Comparing Figure 3 (b) and 3 (c), it is clear that the pores observed in SEM correspond to the polymer-lean droplets that are clearly observed under white light in the optical microscope, and that the basic morphology is preserved during the fracture and solvent extraction steps in preparing SEM samples. Crystallization seems to serve primarily to lock in the liquid phase-separated structure, without altering the basic morphology that is typical of TIPS membranes formed in amorphous polymers. Comparison of Figure 3 (a) and 3 (b) shows that polymer crystallization is primarily confined to the continuous polymer-rich phase. Detailed study of lamellar organization using transmission electron microscopy has been performed by Aerts et al. in similar phase separated solutions.[33]

All structures show that the early stages of L–L demixing have been completed, and the samples have begun to coarsen. The extent of coarsening depends on the amount of time spent in the two-phase liquid region. In both diphenyl ether and diphenyl methane solutions, the pore size may be made significantly smaller by increasing the cooling rate, and hence decreasing the time available for coarsening before crystallization intervenes to lock in the phase separated structure.

At both cooling rates, Figure 3 shows that the solutions in diphenyl methane (e and f) exhibit larger pores than the solutions in diphenyl ether (c and d), despite the fact that the diphenyl ether solutions will spend a greater amount of time in the L–L region of the phase diagram due to their higher cloud point. This may be attributed to the difference in concentration selected for the two solutions. The more concentrated diphenyl ether solutions are expected to have a higher viscosity that would retard

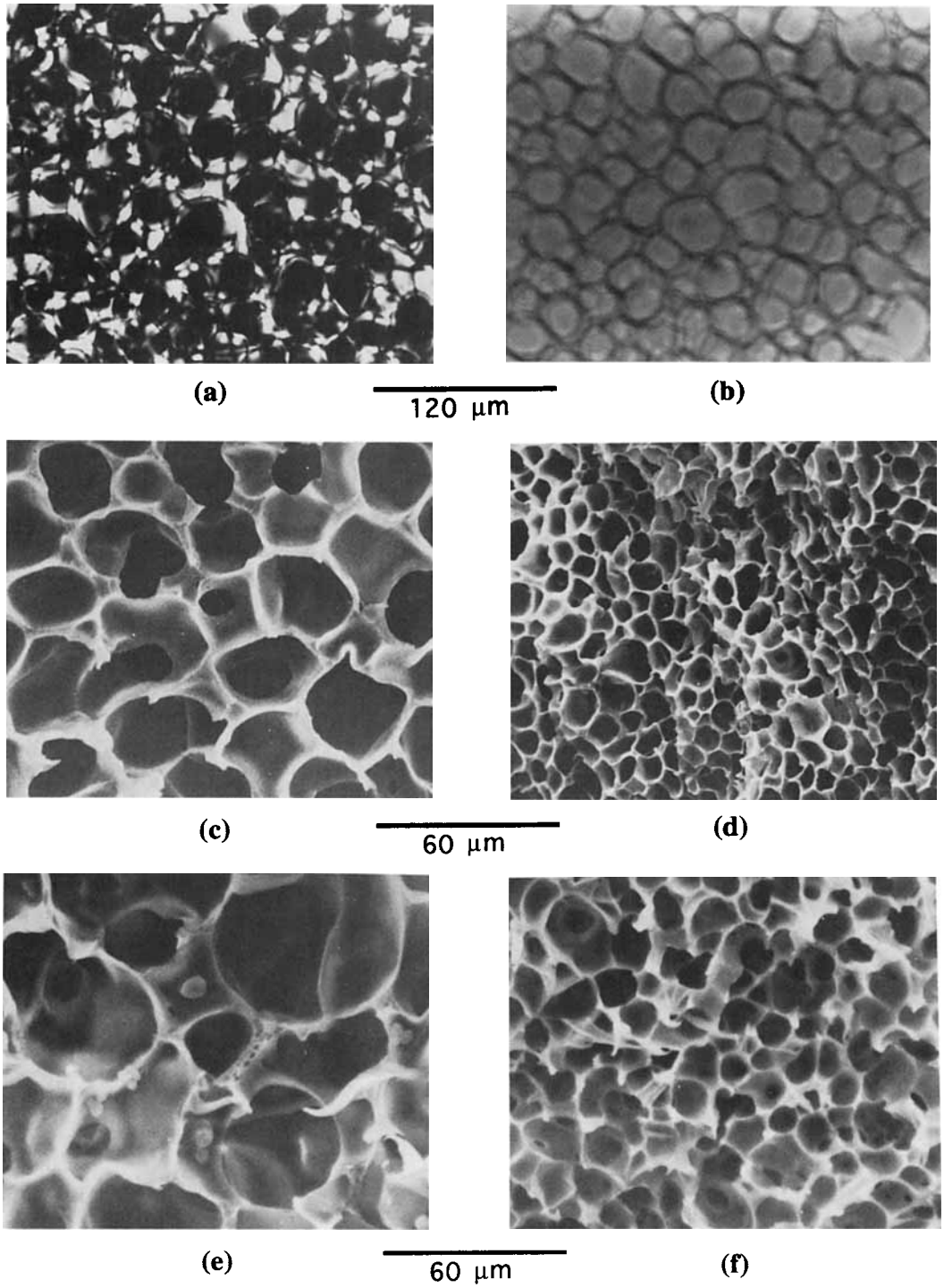

Figure 3 Morphologies observed following ramp cooling. (a, b) Ten percent HPB in diphenyl ether cooled at 10°C/min, observed in the optical microscope at the same sample position under (a) crossed polarizers and (b) white light. (c, d) SEM observation of 10% HPB in diphenyl ether cooled at (c) 10°C/min and (d) 40°C/min. (e, f) SEM observation of 7% HPB in diphenyl methane cooled at (e) 10°C/min and (d) 40°C/min.

coarsening. The effects of concentration are studied in Figure 4 for diphenyl ether solutions at a fixed ramp cooling rate. Coarsening is less pronounced at higher concentrations, due to decreased mobility in the solutions. Comparison of Figure 3(f) and Figure 4(a) shows that at the same concentration and cooling rate, a solution in diphenyl methane exhibits less coarsening than a solution in diphenyl ether, which may be attributed to the larger regime of liquid–liquid phase separation for diphenyl ether solutions (Fig. 2).

Since SEM samples were prepared by ramp cooling in the DSC, it was possible to watch the thermal behavior of the samples during crystallization, and to heat selected samples to study melting behavior. It was found that the low concentration samples exhibited two exothermic peaks during the cooling ramp as shown in Figure 5(a). The first peak was used in constructing the temperature–composition diagram in Figure 2, while the second peak occurred approximately 25°C cooler. On heating, one melting endotherm was seen for all samples at the same temperature for all concentrations. As seen in Figure 5(b), as concentration increased, the relative size of the low temperature peak decreased, until about 12% HPB when the peak was no longer seen. Both solvents yielded similar results, within experimental error.

We attribute the two exothermic peaks to crystallization of the polymer from each of the two discrete liquid phases that should be formed during the ramp cooling in this region of the phase diagram. The low temperature peak would then represent crystallization of the small amount of polymer present in the polymer-lean phase. As overall concentration increases, the fraction of lean phase decreases, resulting in a decrease in the area of the low temperature exothermic peak. Since the polymer-lean phase is itself very dilute, most of the polymer may well be in the polymer-rich phase even when the rich phase is in the minority. Thus, unless the overall concentration is very low, the low temperature peak should be relatively small, as is observed in Figure 5(b).

A mass balance (lever rule) calculation of the fraction of polymer in the dilute phase yields the following expression:

$$f = \frac{\phi_L}{\phi_O}\left(\frac{\phi_R - \phi_O}{\phi_R - \phi_L}\right) \quad (1)$$

where ϕ_O is the overall volume fraction polymer, ϕ_R is the polymer volume fraction in the polymer-rich

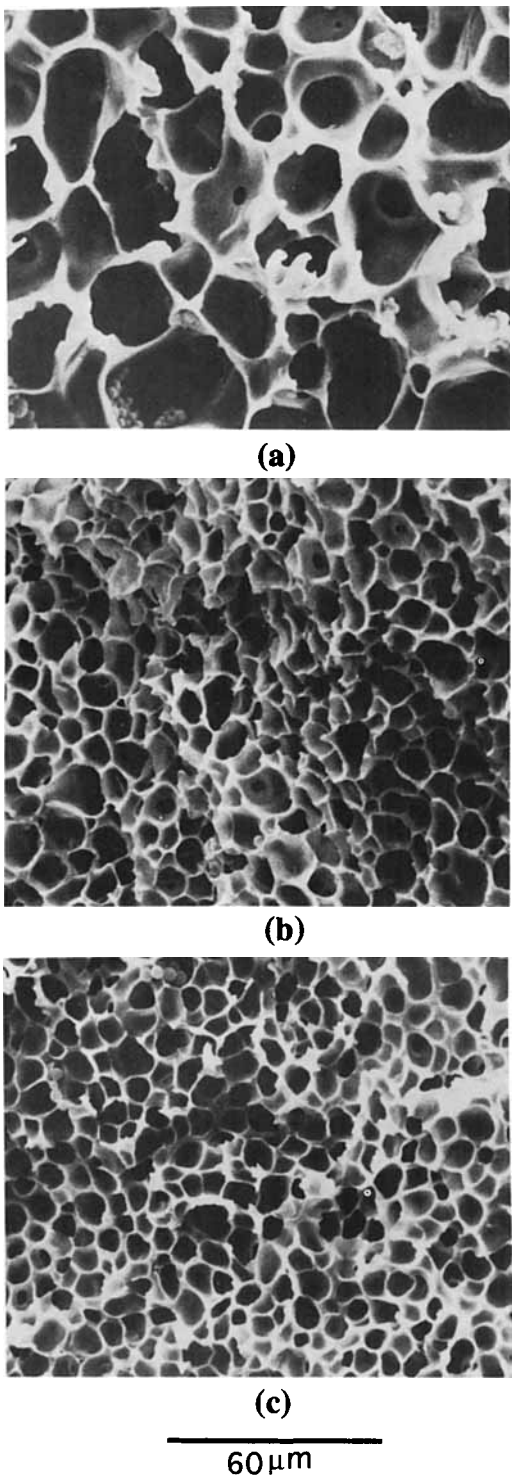

Figure 4 Effects of concentration on structures after ramp cooling. (a) 7%, (b) 10%, and (c) 25% HPB in diphenyl ether cooled at 40°C/min.

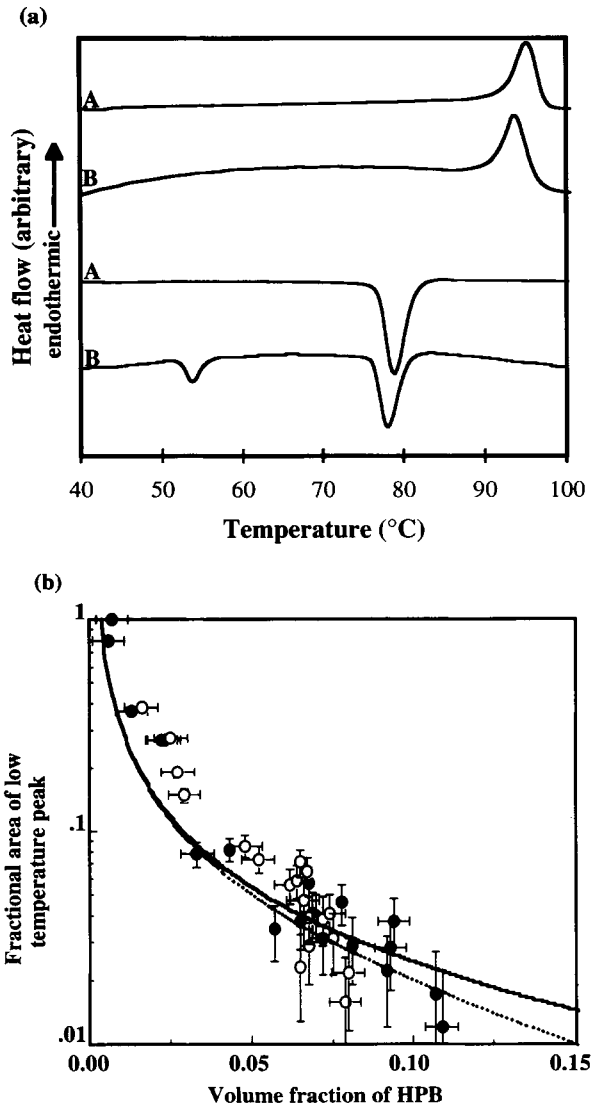

Figure 5 DSC results for ramp cooling. (a) DSC traces for cooling and heating of (A) 30% HPB in diphenyl methane and (B) 3.1% HPB in diphenyl methane. (b) Relative size of low temperature exothermic peak observed during cooling vs polymer concentration. (●) Diphenyl ether solutions; (○) diphenyl methane solutions; (——; - - -) lever rule analysis of eq. (1) for diphenyl ether and diphenyl methane solutions, respectively.

phase, and ϕ_L is the polymer volume fraction in the polymer-lean phase. In order to use this equation to predict how the fractional area of the low temperature peak should depend on overall polymer concentration, it is necessary to assume values for ϕ_R and ϕ_L. From the temperature–composition diagram shown in Figure 2, it possible to estimate ϕ_R. For diphenyl ether, ϕ_R should be approximately 0.55 while for diphenyl methane, ϕ_R is about 0.30. While the predictions of eq. (1) are quite insensitive to the precise value of ϕ_R, the behavior depends more critically on the assumed ϕ_L which is rather difficult to determine precisely. The two values of ϕ_R determined from Figure 2 were used in conjunction with the value $\phi_L = 0.003$ to draw the curves in Figure 5(b). As may be seen, the difference in concentration in polymer-rich phase has little effect on the predicted behavior, and thus it is not surprising that the two solvents should lead to similar experimental data. The general agreement between the data and eq. (1) with reasonable parameters supports the hypothesis that the two peaks reflect crystallization from two discrete liquid phases.

Crystallization from the lean phase occurs at much lower temperatures even though the equilibrium melting point should be identical at the three-phase point. This is probably due to kinetic effects, as both crystal nucleation and growth would be expected to be dramatically slower in such a dilute solution; thus, crystallization at appreciable rates requires much greater undercooling than in the concentrated phase. Another complication may be due to polymer chosen for this study, which contains randomly distributed short ethyl branches. It is believed that these short branches are excluded from the lamellar regions during crystallization.[39,40] It is possible that polymer chains are unevenly distributed between the two liquid phases with respect to branch content, leading to different crystallization behavior in the polymer-lean phase. Effects of the branches during crystallization are observed later during the isothermal experiments, and will be discussed when the DSC results are presented for the isothermally crystallized samples.

In principle, two peaks should be observed throughout the two-phase region, while in practice, no low temperature peaks were observed beyond a polymer volume fraction of around 0.12. As the overall concentration increases, it becomes harder and harder to detect exothermic peaks from the small fraction of polymer present in the dilute phase [leading to significant uncertainty in the data in Fig. 5(b) at higher concentration]. As an example, only about 8 μg of polymer would be present in the dilute phase at a polymer volume fraction of around 0.12, for the DSC sample sizes used in this study. Heats of crystallization of such small amounts of material may be below the detection limit of the instrumentation.

Isothermal Treatments

By the nature of the thermal treatment, liquid–liquid demixing always precedes crystallization dur-

ing ramp cooling, and crystallization serves to lock in the structures resulting from liquid phase separation and coarsening. During isothermal crystallization experiments, however, solutions are rapidly quenched to temperatures between the melting (T_m) and crystallization (T_c) transitions shown in Figure 2, where the two phase separation mechanisms can occur on comparable time scales. Within this region of the phase diagram, crystallization kinetics are a strong function of undercooling. This is illustrated in Figure 6, which shows DSC results for experiments in which a one-phase HPB/diphenyl ether solution was rapidly cooled to a particular temperature, and then heat flow was measured as a function of time, resulting in an exothermic peak as the polymer crystallizes. Even a modest decrease in the crystallization temperature from 90.2 to 88°C causes a pronounced increase in the crystallization rate. DSC experiments at lower crystallization temperatures were thwarted by the inability to establish an isothermal condition before the crystallization was substantially complete; the oil bath quenching procedure used in the preparation of SEM samples is much more rapid than that possible in the calorimeter.

Figure 7 shows typical structures after isothermal crystallization. The rapid temperature quench possible in SEM sample preparation allows lower temperatures to be studied than in the DSC experiments. For each solvent, two temperatures are shown; one is close to T_c, and the other is 5°C higher. Temperatures chosen for Figure 7 include the 3°C temperature difference in melting and crystallization between the two solvents seen in Figure 2. The morphologies observed are very similar to those seen in Figures 3 and 4, dominated by the presence of liquid phase separation. Since the concentrations are near critical, it is reasonable to expect that liquid demixing would be initiated by spinodal decomposition *during* the quench; however, the structures seen in Figure 7 show signs of coarsening, which presumably occurs in parallel with crystallization of the polymer until the phase-separated structure is "locked." Laxminarayan et al.[19] drew similar conclusions for solutions of polypropylene in diphenyl ether by *in situ* observations of the crystallization process with optical microscopy. Samples crystallized at higher temperatures show larger pore sizes. In light of the results in Figure 6, this reflects the fact that crystallization is slower at higher temperatures so that more coarsening can occur before phase separation is arrested. At temperatures much lower than those used in Figure 7, samples crystallize almost immediately upon immersion in the oil bath and have

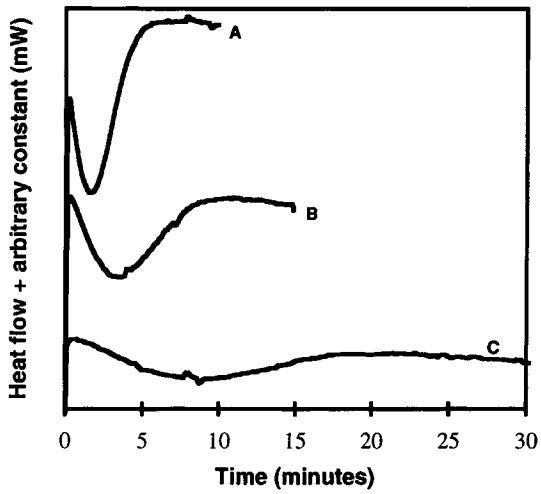

Figure 6 DSC traces for isothermal crystallization in a 10% HPB solution in diphenyl ether. Sample was rapidly cooled from the one phase region to a temperature of (A) 88°C, (B) 89°C, or (C) 90.2°C, and heat flow is measured as a function of time.

very small pore sizes which become independent of the quench depth. Conversely, at conditions much above the upper temperatures used in Figure 7, coarsening progresses to the point that massive coalescence occurs. Thus, there is a fairly small temperature range over which changes in isothermal crystallization rate with undercooling can have a profound impact on the pore sizes in the solidified polymer. Higher concentration samples crystallized at the same temperatures have smaller pore sizes than seen in Figure 7. This may be explained by a decrease in the growth rate of polymer-lean droplets in the polymer-rich matrix.[19,40] This decrease may be explained by a decrease in the quench depth as well as an increase in viscosity as seen earlier.

Since SEM samples were prepared in DSC pans, crystal melting could be investigated calorimetrically in duplicate samples that were prepared using an identical procedure of quenching into an oil bath held at the desired temperature for times sufficient to allow for complete crystallization. DSC experiments were performed at a heating rate of 10°C/min. Typical melting endotherms are shown in Figure 8(a), for the particular case of 10% HPB in diphenyl ether; similar results were obtained for different concentrations in both solvents. It was observed that samples crystallized at lower temperatures (A) displayed a single melting peak. As crystallization temperature was increased (B)–(D) and (F), *two* melting peaks were observed upon heating. The lower peak shifted toward higher melting temperatures as the isothermal crystallization temper-

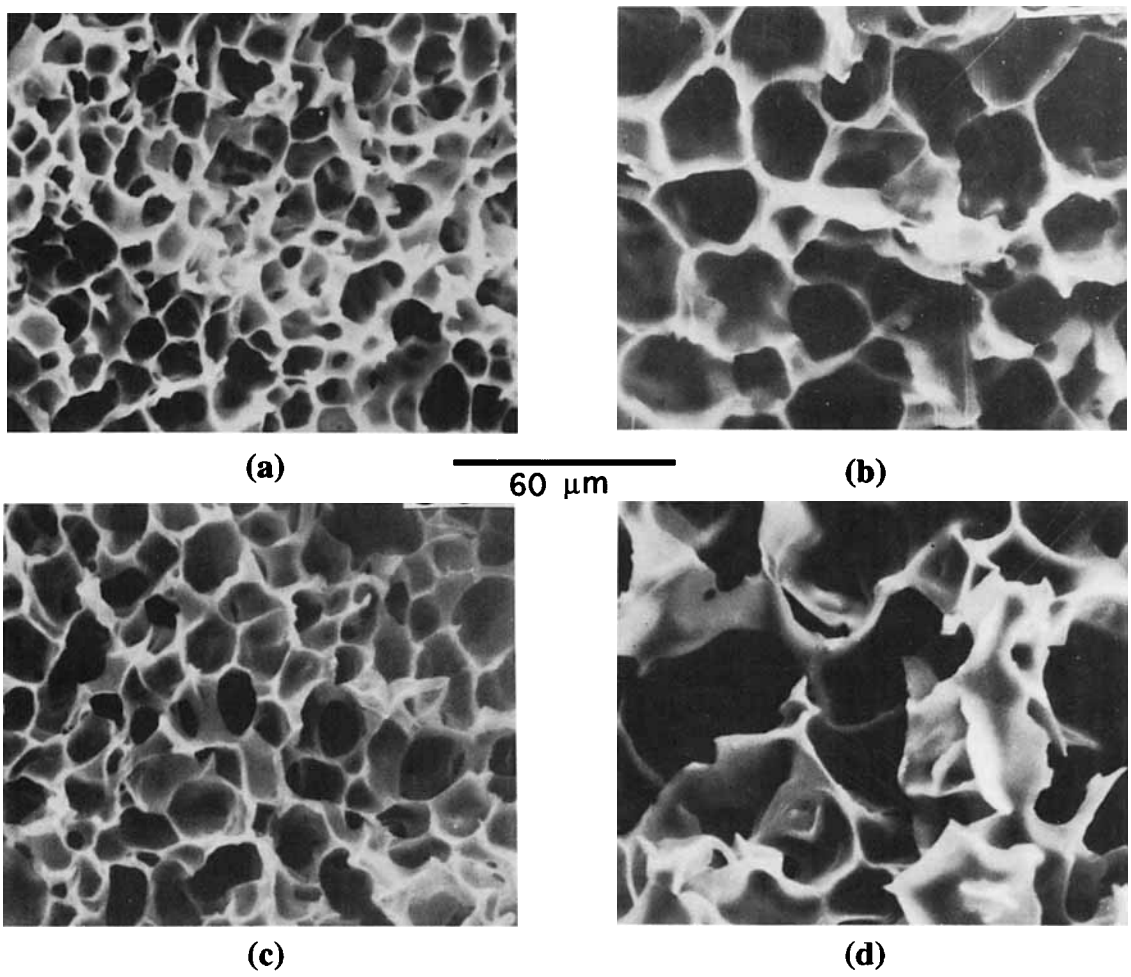

Figure 7 Morphologies observed following isothermal crystallization. Ten percent HPB in diphenyl ether crystallized at (a) 83°C and (b) 88°C; 7% HPB in diphenyl methane crystallized at (c) 80°C and (d) 85°C.

ature increased, while the upper peak was quite insensitive to the crystallization temperature.

Figure 8(b) summarizes melting peak temperatures as a function of isothermal crystallization temperature for two concentrations of HPB solutions in each of the two solvents studied. The dual peak behavior was ubiquitous. In all cases, the upper peak was relatively insensitive to the crystallization temperature, while the lower peak varied considerably and was nearly parallel to the $T_m = T_c$ line. Similar results have been observed when secondary crystallization occurs.[42] It is known that random copolymers melt over a much broader range than other crystalline polymers, and that equilibrium melting temperatures cannot be determined experimentally.[39,43] Forcing a Hoffman–Weeks extrapolation[42] for the higher temperature data in Figure 8(b) would yield an equilibrium melting temperature just a few degrees higher than the observed melting temperature.

One possible explanation for dual peak melting behavior is annealing of imperfect crystals during the 10°C heating ramp, as discussed by Wunderlich.[42] If annealing of the crystals was taking place, heating at faster rates should avoid annealing and would result in an increase in the first peak with a subsequent decrease in the second. For these solutions, heating at faster rates (up to 100°C/min) did not behave in a manner consistent with this explanation. Instead, the first peak appears to decrease in size while the second shifts to higher temperatures. These effects may simply be due to thermal lag artifacts at higher heating rates.

In this case, the dual peak melting behavior may most likely be attributed to the branches in the polymer which hinder crystallization as discussed

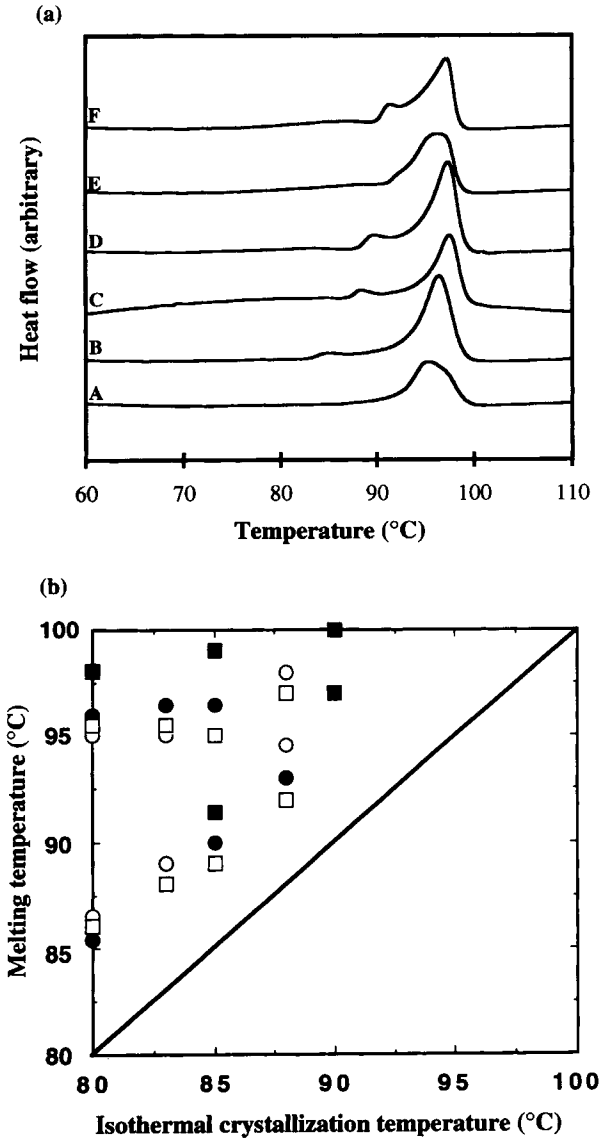

Figure 8 (a) DSC heating curves (10°C/min) for 10% HPB in diphenyl ether crystallized at (A) 50°C, (B) 80°C, (C) 83°C, (D) 85°C, (E) 88°C for 3 min (partial crystallization) and (F) 88°C for 15 min (complete crystallization). (b) Melting peak temperature as a function of crystallization temperature. (●) Ten percent HPB in diphenyl ether; (○) 7% HPB in diphenyl methane; (■) 25% HPB in diphenyl ether; (□) 20% HPB in diphenyl methane.

earlier. Alamo and Mandelkern saw similar dual peak behavior in a hydrogenated poybutadiene which were the result of two populations of crystallite sizes formed during their crystallization procedure.[44] In most polymers, crystallization at higher temperatures generally produces thicker lamella with higher melting temperatures.[42] However, for hydrogenated polybutadiene, the ethyl branches cannot be included in the lamellar region so that crystallinity can actually decrease as isothermal crystallization temperature is increased since more carbon atoms are required to produce the thicker lamellar regions.[45,46] For the same random copolymers studied here, Finerman[46] predicted that only a few additional carbon atoms are required for temperature increases in the range probed here. This would result in melting temperatures which remain fairly constant as seen for the higher peak data for these samples in Figure 8(b). The linear increase in melting temperature of the first peak with increasing isothermal temperature has been seen in samples which undergo secondary crystallization. The increase in size of the first peak observed here may be due to a small increase in carbon atoms required to create lamella at higher temperatures. At the higher temperatures, the branches cause a decrease in crystallinity, but more secondary crystallization may occur on a further decrease in temperature.

Crystallization from One Phase Solutions

In order to demonstrate that the morphologies produced in the preceding sections occur predominantly from liquid phase separation, ramp-cooling experiments were performed on samples which are expected to crystallize from a one-phase solution. This may be accomplished in two ways. Solutions at high concentration of polymer in diphenyl ether or diphenyl methane should crystallize from a single phase liquid; a similar approach was used by Lloyd and co-workers.[11-18] Alternatively, a better solvent could be chosen in which no region of liquid instability is expected on the phase diagram. Here we report results on 55% HPB in diphenyl methane and 30% HPB in xylene to compare results for the two approaches.

Structures prepared by ramp cooling at 10°C/min are shown in Figure 9 for both solutions. The 55% solution of HPB in diphenyl methane shows clear evidence of both crystallization and liquid phase separation, despite its high concentration. From Figure 2, it is clear that a 55% solution in diphenyl methane is well to the right of the binodal curve in the temperature range in which DSC shows that the polymer is crystallizing. Along with the qualitative differences between this morphology and that seen for instance in Figure 3, this suggests that the mechanism of phase separation is fundamentally different in these two cases, despite the evidence for liquid phase separation in both cases. In solutions at lower concentration, crystallization occurs within a morphological template dictated by the liquid

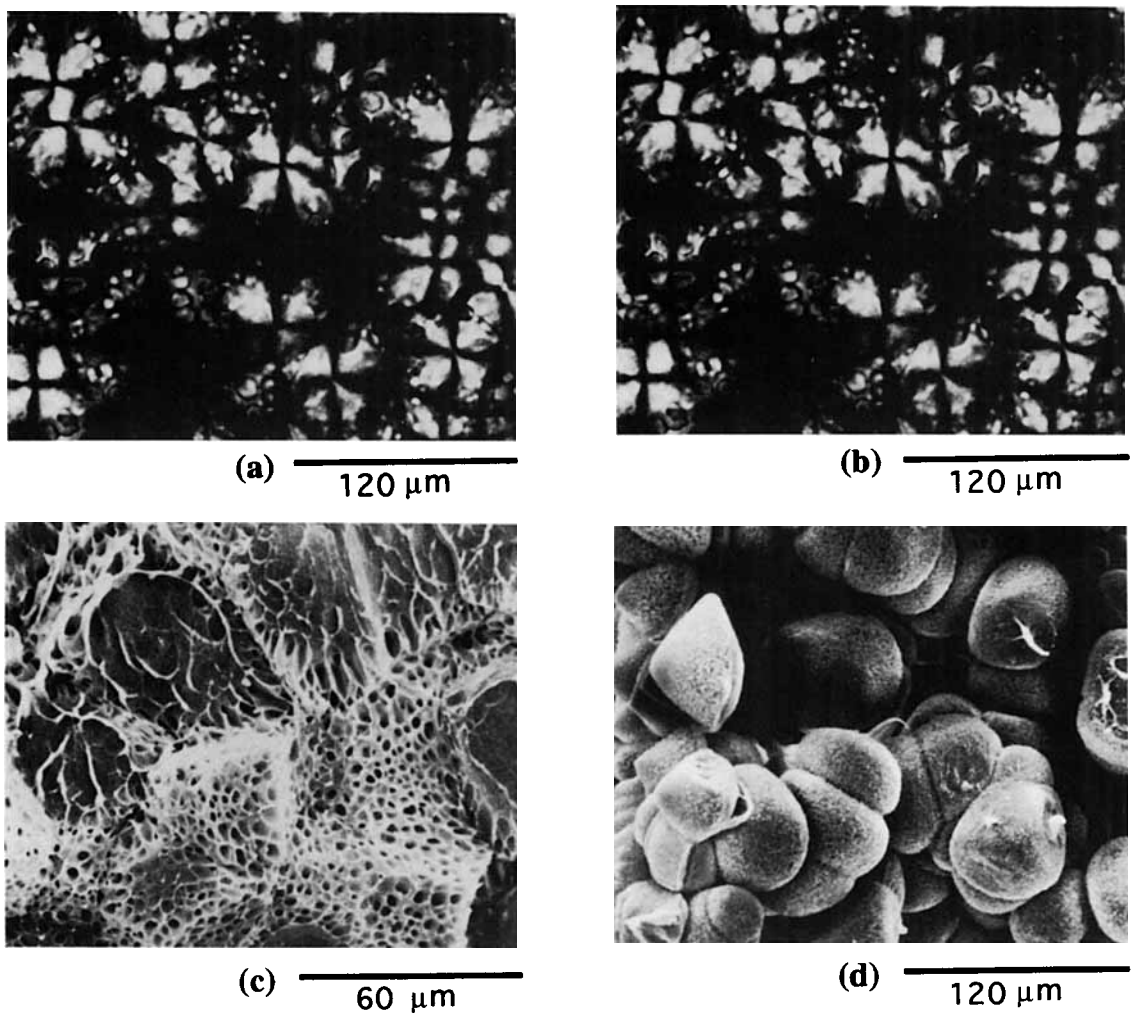

Figure 9 Morphologies observed resulting from crystallization in one phase solution during ramp cooling at 10°C/min: 55% HPB in diphenyl methane, observed via optical microscopy with (a) crossed polarizers or (b) white light, and observed via (c) SEM; (d) 30% HPB in xylene observed via SEM. Micrographs in (a) and (b) show identical field of view.

phase separation that precedes it. For 55% HPB in diphenyl methane, the opposite seems to be true. In Figure 9(a), it is clear that very well defined spherulites have grown. Comparing with Figure 9(b), the regions of liquid phase separation are confined to the space between spherulites. A similar conclusion is drawn from the SEM micrograph in Figure 9(c). This suggests that liquid phase separation occurs subsequent to the growth of the spherulites.

The morphology observed in Figure 9(a–c) may be rationalized in terms of rejection of diluent from the crystal growth front as described by Keith and Padden,[47] who investigated spherulitic growth in solutions. They found that diluents of low molecular weight could diffuse away from the growing spherulite causing nonvolume filling spherulitic structures. This also results in enhanced concentration of diluent in the interstitial spaces between spherulites. Tanaka and Nishi argue that formation of diluent-rich layers at spherulite growth fronts is responsible for their observation of liquid phase separation induced at the edges of poly(ϵ-caprolactone) spherulites in a blend with oligomeric polystyrene diluent.[48] The interfacial diluent concentration in this layer is sufficiently high that the solution is locally within the regime of liquid phase separation. The structures presented here are very similar to their observations, except that the liquid demixing appears *throughout* the interspherulitic regions. This implies that solvent diffusion is sufficiently rapid

relative to spherulitic growth that the diluent rejected by the growing spherulites is quickly spread through the entire interspherulitic region, eventually causing the concentration in this region to reach the two phase region.

The preceding results show that liquid phase separation may still influence morphology in poor solvents even when the concentration is sufficiently high that crystallization should be the primary phase separation mechanism. In the 30% solution of HPB in xylene, liquid phase separation should be strictly excluded, since there is no regime of liquid phase separation anywhere in the equilibrium phase diagram. Indeed, the resulting morphology consists of spherulites that are clearly observed between crossed polarizers, and which SEM reveals to be essentially isolated from one another, as seen in Figure 9(d). This micrograph is typical of structures obtained when crystallizing from a one-phase polymer solution.[11,17,23,47,49] This morphology is very distinct from the interconnected structures with potential membrane applications that result when liquid demixing plays a role in the phase separation process.

SUMMARY

In solutions of crystallizable polymer in a poor solvent, the presence of multiple types of phase behavior complicates consideration of processes in which porous polymers with potential membrane applications are produced through controlled phase separation. At low concentration, samples subjected to either ramp cooling or isothermal crystallization exhibited morphologies that principally reflect liquid demixing followed by coarsening, leading to a porous structure similar to those produced from amorphous polymer solutions. Crystallization serves primarily to lock in the liquid phase-separated structure at a particular level of maturity. In this light, an important process variable is the amount of time allowed for coarsening before crystallization arrests further evolution of the phase-separated structure. Larger pores result from lower cooling rates in ramp cooling, and from higher isothermal crystallization temperatures. In the latter case, small changes in temperature have a large influence on pore size, since crystallization rates vary dramatically as a function of undercooling. DSC experiments during ramp cooling exhibit two exothermic peaks, reflecting crystallization of polymer from two discrete liquid phases. Isothermally crystallized samples, conversely, exhibit two endothermic DSC peaks in melting experiments, which has been attributed to the rejection of ethyl branches during crystallization. Finally, highly concentrated samples show a peculiar phase-separated morphology in which liquid phase separation appears to have been induced at the growth fronts of spherulites crystallizing from what otherwise would have been a single-phase solution.

Acknowledgment is made to the Donors of The Petroleum Research Fund, administered by the American Chemical Society, for the support of this research. We thank Professor B. Crist for assistance with polymer synthesis.

REFERENCES

1. R. E. Kesting, *Synthetic Polymer Membranes,* Wiley, New York, 1985.
2. J. A. Castro, U.S. Pat. 4 247 498, Jan. 27, 1981.
3. G. T. Caneba and D. S. Soong, *Macromolecules,* **18,** 2538 (1985).
4. G. T. Caneba and D. S. Soong, *Macromolecules,* **18,** 2545 (1985).
5. J. H. Aubert and R. L. Clough, *Polymer,* **26,** 2047 (1985).
6. J. Arnauts and H. Berghmans, *Polym. Commun.*, **28,** 66 (1987).
7. R. M. Hikmet, S. Callister, and A. Keller, *Polymer,* **29,** 1378 (1988).
8. F. J. Tsai and J. M. Torkelson, *Macromolecules,* **23,** 775 (1990).
9. F. J. Tsai and J. M. Torkelson, *Macromolecules,* **23,** 4983 (1990).
10. J. H. Aubert, *Macromolecules,* **23,** 1446 (1990).
11. D. R. Lloyd, K. E. Kinzer, and H. S. Tseng, *J. Membrane Sci.,* **52,** 239 (1990).
12. G. B. A. Lim, S. S. Kim, Q. Ye, Y. F. Wang, and D. R. Lloyd, *J. Membrane Sci.,* **64,** 31 (1991).
13. S. S. Kim, G. B. A. Lim, A. A. Alwattari, Y. F. Wang, and D. R. Lloyd, *J. Membrane Sci.,* **64,** 41 (1991).
14. A. A. Alwattari and D. R. Lloyd, *J. Membrane Sci.,* **64,** 55 (1991).
15. K. S. McGuire, D. R. Lloyd, and G. B. A. Lim, *J. Membrane Sci.,* **79,** 27 (1993).
16. D. R. Lloyd, J. W. Barlow, and K. E. Kinzer, in *New Membrane Materials and Processes for Separation,* K. K. Sirkar and D. R. Lloyd, Eds., AIChE Symp. Ser. No. 261, American Institute of Chemical Engineers, New York, 1988, p. 28.
17. S. S. Kim and D. R. Lloyd, *J. Membrane Sci.,* **64,** 13 (1991).
18. D. R. Lloyd, S. S. Kim, and K. E. Kinzer, *J. Membrane Sci.,* **64,** 1 (1990).
19. A. Laxminarayan, K. S. McGuire, S. S. Kim, and D. R. Lloyd, *Polymer,* **35,** 3060 (1994).
20. K. S. McGuire, A. Laxminarayan, and D. R. Lloyd, *Polymer,* **35,** 4404 (1994).
21. A. J. Reuvers, F. W. Altena, and C. A. Smolders, *J. Polym. Sci.: Part B: Polym. Phys.,* **24,** 793 (1986).

22. W. R. Burghardt, L. Yilmaz, and A. J. McHugh, *Polymer,* **28,** 2085 (1987).
23. A. M. W. Bulte, B. Folkers, M. H. V. Mulder, and C. A. Smolders, *J. Appl. Polym. Sci.,* **50,** 13 (1993).
24. W. R. Burghardt, *Macromolecules,* **22,** 2482 (1989).
25. R. B. Richards, *Trans. Faraday Soc.,* **42,** 10 (1946).
26. P. J. Flory, L. Mandelkern, and H. K. Hall, *J. Am. Chem. Soc.,* **73,** 2532 (1951).
27. J. Nakajima, H. Fujiwara, and F. Hamada, *J. Polym. Sci., Polym. Phys. Ed.,* **4,** 507 (1966).
28. J. Nakajima and H. Fujiwara, *J. Polym. Sci., Polym. Phys. Ed.,* **6,** 723 (1966).
29. P. Schaaf, P. Lotz, and J. C. Whitman, *Polymer,* **28,** 193 (1987).
30. G. Chui and L. Mandelkern, *Macromolecules,* **23,** 5356 (1990).
31. H. K. Lee, A. S. Myerson, and K. Levon, *Macromolecules,* **25,** 4002 (1992).
32. W. Stoks and H. Berghmans, *J. Polym. Sci.: Part B: Polym. Phys.,* **29,** 609 (1991).
33. L. Aerts, M. Kunz, H. Berghmans, and R. Koningsveld, *Makromol. Chem.,* **194,** 2697 (1993).
34. S. S. Kim and D. R. Lloyd, *Polymer,* **33,** 1047 (1992).
35. J. H. Aubert, *Macromolecules,* **21,** 3468 (1988).
36. T. M. Krigas, J. M. Carella, M. J. Struglinski, B. Crist, W. W. Graessley, and F. C. Schilling, *J. Polym. Sci. Part B: Polym. Phys.,* **23,** 509 (1985).
37. J. Mays, N. Hadjichristidis, and L. J. Fetters, *Macromolecules,* **17,** 2723 (1984).
38. H. Rachapudy, G. G. Smith, V. R. Raju, and W. W. Graessley, *J. Polym. Sci., Polym. Phys. Ed.,* **17,** 1211 (1979).
39. A. Keller and D. Priest, *J. Polym Sci. Part B,* **8,** 13 (1970).
40. R. G. Alamo, E. K. M. Chan, L. Mandelkern, and I. G. Voigt-Marten, *Macromolecules,* **25,** 6381 (1992).
41. S. W. Song and J. M. Torkelson, *Macromolecules,* **27,** 6389 (1994).
42. B. Wunderlich, *Macromolecular Physics: 3 Crystal Melting,* Academic Press, New York, 1980.
43. L. Lu, R. G. Alamo, and L. Mandelkern, *Macromolecules,* **27,** 6571 (1994).
44. R. Alamo, and L. Mandelkern, *J. Polym. Sci. Part B: Polym. Phys.,* **24,** 2087 (1986).
45. T. Pakula, *Polymer,* **23,** 1300 (1982).
46. T. M. Finerman, Ph.D. Dissertation, Northwestern University, 1990.
47. H. D. Keith and F. J. Padden Jr., *J. Appl. Phys.,* **35,** 1270 (1964).
48. H. Tanaka and T. Nishi, *Phys. Rev. E,* **39,** 783 (1989).
49. A. Prasad, H. Marand, and L. Mandelkern, *J. Polym. Sci. Part B: Polym. Phys.,* **31,** 1819 (1993).

Received January 11, 1995
Accepted March 20, 1995